Pergamon

Computers & Fluids Vol. 27, No. 3, pp. 367–380, 1998

Printed in Great Britain
PII: S0045-7930(97)00041-8
0045-7930/98 $19.00 + 0.00

PULSATILE BLOOD FLOW IN A PIPE

GIUSEPPE PONTRELLI[1]

[1]Istituto per le Applicazioni del Calcolo (CNR), Viale del Policlinico, 137, 00161 Rome, Italy

(Received 13 January 1997; revised 18 January 1997)

Abstract—The unsteady flow of blood in a straight, long, rigid pipe, driven by an oscillatory pressure gradient is studied. Three different non–newtonian models for blood are considered and compared. One of them turns out to offer the best fit of experimental data, when the rheological parameters are suitably fixed. Numerical results are obtained by a spectral collocation method in space and the implicit trapezoidal finite difference method in time. © 1998 Elsevier Science Ltd. All rights reserved

1. INTRODUCTION

The desire to understand the flow of blood through the cardiovascular system and prosthetic devices has stimulated a lot of research activity in hemodynamics. Such studies are of particular importance because there is indirect evidence that the cause and the developments of many cardiovascular diseases are, to a great extent, related to the characteristics of blood flow, such as the high values of the shear stress at the wall or its variation [1–4].

The study of the rheological properties of blood can allow a better understanding of blood circulation. The latter depends on numerous factors such as the driving force of the heart, the shape, as well as mechanical and physiological behaviour of the vascular walls [1,5–8].

Blood is a suspension of different cells in a liquid, the plasma: the red cells are by far the most numerous and it is generally assumed that their influence in blood rheology is predominant: although plasma is constituted by 90% water, it is commonly accepted that blood is a non-newtonian fluid because the elastic and deformable structure of red cells gives to it a shear dependent viscosity and a viscoelastic nature [7,9–15].

In this work, however, the liquid *blood* is considered as a continuum medium. Such an approach allows the use of physical principles of conservation of mass and momentum to be applied to the bulk fluid and gives meaning to such measured variables as pressure, velocity, wall shear stress and so on. In the continuum approach, phenomena of interest are governed by large distances and times compared to the dimension of a red cell or its characteristic rotation time. The constitutive equation of blood is determined essentially by the plasma viscosity, the flexibility of red cells, and the characteristics of this interaction. Due to the complex nature of blood, a theoretical universal reliable model in the mechanics of continuum is still lacking. Many different factors may influence the behaviour of blood flow and make this attempt difficult: for example, properties of blood strongly depend upon the hematocrit, a parameter which differs between people and can change in an individual by a significant amount, even due to effects of illness and of temperature [10,11,16,17].

Nevertheless, many mathematical models for describing rheological behaviour of blood have been extensively developed in recent years [6,9,10,13,18,19].

Though a great effort has been invested in steady flows [14,17], very little is known, however, anout blood rheology in unsteady flows. Actually in a living body the heart generates a pulsatile flow and its fluctuations are progressively damped owing to the elasticity of the major arteries; however, the periodic nature of the blood flow is observed in smaller vessels and arterioles where the distensibility of the walls is much less and the influence of pulsation frequency becomes more important. Walls of such vessels can be considered sufficiently rigid and the flow will be solely determined by the pressure gradient. Knowledge of the magnitude and variation

of the wall shear stress in an arterial segment is useful in understanding the disease of blood vessels, and constitutes an important hemodynamic factor [3,16,20].

Because of the limitation of experimental methods in oscillatory flows, mathematical models and numerical simulation play a crucial role in the analysis of the flow and may give useful additional information, particularly when the geometry is complicated such as in the arterial flow.

The purpose of this work is to compare the behaviour of three mathematical models for blood: the first two of them are able to capture some of the physical properties of blood in pulsatile flow and the third one, recently proposed in [21,22], is a combination of them. Actually, although it has been well established that blood is both a viscoelastic and a shear-thinning fluid, the meaning and the magnitude of the rheological parameters have not been yet clarified. Due to the high nonlinear behaviour of these non–newtonian models, some appropriate simplification on the flow is necessary. Here we considered the one-dimensional laminar flow in a pipe of infinite length, in the axisymmetric approximation, with a known, pulsatile pressure gradient. Although this flow appears to be oversimplified and unrealistic to describe the blood circulation, nevertheless, as a prototype, it is extremely useful to set up the model and to understand its main characteristic features, in view of more complex applications.

Other mathematical models for unsteady pipe flows with pressure gradients of different type have been developed and solved analytically or numerically [13,18,23–28].

For all the models presented, the motion equations express a nonlinear coupling between stress and velocity fields and have to be solved numerically. The spatial operator is first linearized and then solved by a collocation spectral method over the Legendre Gauss–Lobatto points.

The linear time operator is solved by a trapezoidal finite difference method. The flow dependence on the dimensionless parameters has been investigated carefully. The numerical results obtained by integrating the momentum equations have been compared first with the analytical solution available for the newtonian fluid [29] or for the Maxwell fluid [25], and then with other numerical studies in literature: similarities have been pointed out and differences discussed.

2. MATHEMATICAL MODELS

It is generally accepted that the newtonian assumption for the constitutive nature of blood is adequate only for flow in larger vessels. However, at low shear rates ($< 100\ s^{-1}$) as well as in flows in smaller vessels, blood flow is not well described by the Navier–Stokes model [7,16,17]. Actually the average shear rate at the wall of arteries is greater than this, and we shall assume blood to be newtonian in that region. Nevertheless, near the center of the vessel, or in separated regions of recirculating flow, the average value of shear rate will be small. Furthermore, in pulsatile flows, the wall shear stress vanishes twice per cycle, and there are instants where it is considerably small.

In the last decades, many mathematical models have been studied to set a reliable constitutive equation for blood, in the attempt to model either the nonlinear dependence of the viscosity on the strain rate, and the viscoelastic effects such as stress relaxation [6,13,19,31,32]. Due to the variable behaviour and the complex chemical structure of this liquid, none of the constitutive equations studied so far seems to be completely satisfactory for all kinds of flow regimes. Recently, a new model is being developed for blood [21,22]: in the following we study separately the two components it has been built up, each of them being able to predict some particular properties, in order to understand the role of the different concurrent forces on the flow.

The Cauchy stress tensor $\mathbf{T}$ is split into an isotropic part due to the pressure p and an extra-stress $\mathbf{S}$:

$$\mathbf{T} = -p\mathbf{I} + \mathbf{S} \tag{1}$$

While the plasma is a fluid with no significant departure from newtonian behaviour, when red cells are present in plasma the viscosity of the whole mixture increases considerably. Marked non-newtonian properties are evidenced for concentrations $> 10\%$ [16]. When the value of hematocrit is held fixed and shear stress is plotted vs shear rate it turns out that the viscosity is not a constant, but a decreasing function as depicted in Fig. 1. This leads to the following:

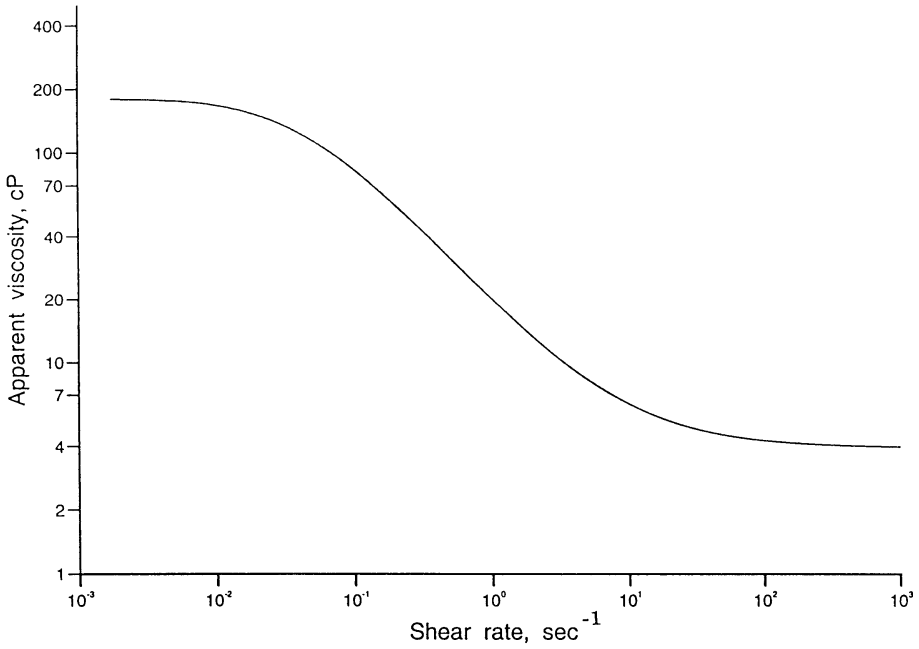

Fig. 1. The shear rate dependent viscosity function [Equation (3)].

2.1. Generalized newtonian model (GN)

$$\mathbf{S} = \mu(\mathbf{A}_1)\mathbf{A}_1 \tag{2}$$

with:

$$\mathbf{A}_1 = \mathbf{L} + \mathbf{L}^T \qquad \mathbf{L} = \text{grad } \mathbf{v}$$

and

$$\mu(\mathbf{A}_1) = \eta_\infty + (\eta_0 - \eta_\infty)\left[\frac{1 + \log(1 + \Lambda\dot{\gamma})}{1 + \Lambda\dot{\gamma}}\right] \qquad \dot{\gamma} = \left[\frac{1}{2}\text{tr}(\mathbf{A}_1^2)\right]^{\frac{1}{2}} \tag{3}$$

η_0, η_∞ are the asymptotic apparent viscosity as $\dot{\gamma} \to 0$ and ∞ respectively, ($\eta_0 > \eta_\infty$), and $\Lambda \geqslant 0$ a material constant with the dimension of time representing the degree of shear-thinning [for $\Lambda = 0$ $\mu(\mathbf{A}_1) = \eta_0 =$const. and the model reduce to the newtonian one]. The complex nature of blood is approximated here with a three-parameter shear-thinning model, where the apparent viscosity is expressed as a decreasing function of the shear rate. At low shear rates, the apparent viscosity increases considerably. The asymptotic values η_0 and η_∞ are common in many other inelastic shear-thinning models [18,19,24] and their values have set up through experiments (see Fig. 1) [7]. This is a first attempt to modify the newtonian model for blood with the introduction of a shear rate dependent viscosity.

2.2. Oldroyd-B model (OB)

$$\mathbf{S} + \lambda_1(\dot{\mathbf{S}} - \mathbf{LS} - \mathbf{SL}^{\mathrm{T}}) = \mu(\mathbf{A}_1 + \lambda_2(\dot{\mathbf{A}}_1 - \mathbf{LA}_1 - \mathbf{A}_1\mathbf{L}^{\mathrm{T}})) \tag{4}$$

with μ is a constant viscosity, λ_1 and λ_2 two constants having the dimension of time, referred to as relaxation and retardation time respectively.†

†The dot over a variable f (scalar, vector or tensor) denotes the material derivative as in: $\dot{f} = (\partial f)/(\partial t) + \mathbf{v}$ grad f.

The constitutive Equation (4) includes the stress relaxation, the creep and the normal stress effects exhibited by blood, but a constant viscosity. Experimental results show that, mostly in unsteady flows, blood possesses significant viscoelastic properties [9–11].

Since models GN and OB are representative for two different and independent properties of the blood, the idea to put them together is in the following:

2.3. Generalized Oldroyd-B model (GOB)

$$\mathbf{S} + \lambda_1(\dot{\mathbf{S}} - \mathbf{LS} - \mathbf{SL}^{\mathrm{T}}) = \mu(\mathbf{A}_1)\mathbf{A}_1 + \eta_0\lambda_2(\dot{\mathbf{A}}_1 - \mathbf{LA}_1 - \mathbf{A}_1\mathbf{L}^{\mathrm{T}}) \tag{5}$$

where $\mu(\mathbf{A}_1)$ is given by Equation (3). Since it is the combination of the GN and OB models, it captures the characteristics of both and it is expected to give the best fit of experimental data.

All the models reduce to the newtonian one for some values of the material parameters. The use of these mathematical models turns out to be very sensitive to the choice of the material parameters. This is a delicate task and deserves a further investigation in a following study.

3. FLOW EQUATIONS

Let us consider the flow of blood in a straight long† pipe of circular cross section having radius R. Blood is assumed to be an isotropic, homogeneous and incompressible continuum, having constant density‡ ρ, and the vessel walls are considered rigid and impermeable (see Introduction).

The motion equation is:

$$\rho\frac{\partial \mathbf{v}}{\partial t} + \mathbf{v}\cdot\nabla\mathbf{v} = \operatorname{div}\mathbf{T} \tag{6}$$

where $\mathbf{v} = (u, v, w)$ is the velocity vector and the external forces are supposed negligible.

Let us now consider a cylindrical coordinate system (r, θ, z) having the z-axis coincident with the pipe axis. In the hypothesis of laminar flow, the only nonzero component of velocity is w. Moreover, since the flow is assumed to be axisymmetric, the fluid dynamical variables do depend on r only, except for the pressure which depends on z only. In such hypothesis the convective term in Equation (6) vanishes.

In the cardiovascular system, the motion of the blood is driven by a local pressure gradient along the longitudinal direction of the vessel, which in turn is determined by the propagation of the heart pressure pulse. It is worth noting that the pressure, being essentially periodic, can be subjected to Fourier series analysis. Therefore, for the sake of simplicity, it is assumed that the pressure gradient is known as a function of time:

$$-\frac{1}{\rho}\frac{\partial p}{\partial z} = A\cos(\omega t) \quad 0 \leqslant t \leqslant T \tag{7}$$

Any other complex periodic function, such as the arterial pulse, can be represented in terms of Equation (7) by a Fourier series.

In case of GN, the constitutive Equation (2), substituted in Equation (1) and in the motion Equation (6), gives:

$$\rho\frac{\partial w}{\partial t} = -\frac{\partial p}{\partial z} + \left[\eta_\infty + (\eta_0 - \eta_\infty)\frac{1+\log\sigma}{\sigma}\right]\frac{1}{r}\frac{\partial w}{\partial r} + \left[\eta_\infty + (\eta_0 - \eta_\infty)\left(\frac{1+\log\sigma}{\sigma} - \frac{\Lambda\left|\frac{\partial w}{\partial r}\right|\log\sigma}{\sigma^2}\right)\right]\frac{\partial^2 w}{\partial r^2} \tag{8}$$

†Here *long* means of length large enough compared with the radius of the pipe.

‡Blood cannot be regarded as a homogeneous fluid in the smallest blood vessels, because the diameters and spacing of red cells are comparable with the capillary diameter. However, in vessels with diameter $> 100\,\mu$m, it can be effectively considered as a homogeneous fluid, because the scale of the microstructure is much smaller than that of the flow.

where:

$$\sigma = 1 + \Lambda \left| \frac{\partial w}{\partial r} \right|$$

In case OB, the motion equation is coupled with the constitutive equation components:

$$\begin{aligned} \rho \frac{\partial w}{\partial t} &= -\frac{\partial p}{\partial z} + \frac{\partial S_{rz}}{\partial r} + \frac{S_{rz}}{r} \\ S_{rz} + \lambda_1 \frac{\partial S_{rz}}{\partial t} &= \mu \left(\frac{\partial w}{\partial r} + \lambda_2 \frac{\partial^2 w}{\partial r \partial t} \right) \\ S_{zz} + \lambda_1 \left(\frac{\partial S_{zz}}{\partial t} - s \frac{\partial w}{\partial r} S_{rz} \right) &= -2\mu\lambda_2 \left(\frac{\partial w}{\partial r} \right)^2 \end{aligned} \tag{9}$$

Similarly, in the case of GOB, we get the following set of nonlinear equations:

$$\begin{aligned} \rho \frac{\partial w}{\partial t} &= -\frac{\partial p}{\partial z} + \frac{\partial S_{rz}}{\partial r} + \frac{S_{rz}}{r} \\ S_{rz} + \lambda_1 \frac{\partial S_{rz}}{\partial t} &= \left[\eta_\infty + (\eta_0 - \eta_\infty) \frac{1 + \log \sigma}{\sigma} \right] \frac{\partial w}{\partial r} + \eta_0 \lambda_2 \frac{\partial^2 w}{\partial r \partial t} \\ S_{zz} + \lambda_1 \left(\frac{\partial S_{zz}}{\partial t} - 2 \frac{\partial w}{\partial r} S_{rz} \right) &= -2\eta_0 \lambda_2 \left(\frac{\partial w}{\partial r} \right)^2 \end{aligned} \tag{10}$$

The boundary conditions associated to the physical problem are given by:

$$w = 0 \quad \text{at} \quad r = R \tag{11}$$

(no slip velocity at the wall) and

$$\frac{dw}{dr} = 0 \quad \text{at} \quad r = 0 \tag{12}$$

(axisymmetry). Any initial condition consistent with Equations (11) and (12) does not affect the solution, apart from a short transient.

Though Equations (10) reduces to Equations (9) for $\Lambda = 0$, and to Equation (8) for $\lambda_1 = \lambda_2 = 0$, each of the three models has its own characteristics and may require a special treatment. For example, GN formally exhibits a lesser number of variables but, as a counterpart, a spatial derivative one order greater than OB and GOB, and has to be solved separately.

By introducing the following change of variables:

$$\begin{aligned} & r \rightarrow \frac{r}{R} \quad z \rightarrow \frac{z}{R} \quad t \rightarrow \frac{Wt}{R} \\ & p \rightarrow \frac{p}{\rho W^2} \quad w \rightarrow \frac{w}{W} \quad S_{rz} \rightarrow \frac{S_{rz}}{\rho W^2} \quad S_{zz} \rightarrow \frac{S_{zz}}{\rho W^2} \end{aligned}$$

with W a characteristic velocity and by defining the following dimensionless constants:

$$\begin{aligned} & \mathrm{Re} = \frac{RW}{\nu} \quad \gamma = \frac{\eta_\infty}{\eta_0} \quad A^* = \frac{AR}{W^2} \quad T^* = \frac{TW}{R} \\ & \lambda_1^* = \frac{\lambda_1 W}{R} \quad \lambda_2^* = \frac{\lambda_2 W}{R} \quad \Lambda^* = \frac{\Lambda W}{R} \quad \omega^* = \frac{\omega R}{W} \end{aligned}$$

with $\nu = \eta_0/\rho$ ($\nu = \mu/\rho$ in the OB case) the kinematic viscosity, the Equation (8), the systems (9)

and (10) are nondimensionalized respectively as:

$$\frac{\partial w}{\partial t} = -\frac{\partial p}{\partial z} + \frac{1}{\mathrm{Re}}\left\{\left[\gamma + (1-\gamma)\frac{1+\log\delta}{\delta}\right]\frac{1}{r}\frac{\partial w}{\partial r} + \left[\gamma + (1-\gamma)\left(\frac{1+\log\delta}{\delta} - \frac{\Lambda^*\left|\frac{\partial w}{\partial r}\right|\log\delta}{\delta^2}\right)\right]\frac{\partial^2 w}{\partial r^2}\right\} \quad (13)$$

where:

$$\delta = 1 + \Lambda^*\left|\frac{\partial w}{\partial r}\right|$$

$$\frac{\partial w}{\partial t} = -\frac{\partial p}{\partial z} + \frac{\partial S_{rz}}{\partial r} + \frac{S_{rz}}{r} \quad (14)$$

$$S_{rz} + \lambda_1^*\frac{\partial S_{rz}}{\partial t} = \frac{1}{\mathrm{Re}}\left(\frac{\partial w}{\partial r} + \lambda_2^*\frac{\partial^2 w}{\partial r \partial t}\right) \quad (15)$$

$$S_{zz} + \lambda_1^*\left(\frac{\partial S_{zz}}{\partial t} - 2\frac{\partial w}{\partial r}S_{rz}\right) = -2\frac{\lambda_2^*}{\mathrm{Re}}\left(\frac{\partial w}{\partial r}\right)^2 \quad (16)$$

and

$$\frac{\partial w}{\partial t} = -\frac{\partial p}{\partial z} + \frac{\partial S_{rz}}{\partial r} + \frac{S_{rz}}{r} \quad (17)$$

$$S_{rz} + \lambda_1^*\frac{\partial S_{rz}}{\partial t} = \frac{1}{\mathrm{Re}}\left\{\left[\gamma + (1-\gamma)\frac{1+\log\delta}{\delta}\right]\frac{\partial w}{\partial r} + \lambda_2^*\frac{\partial^2 w}{\partial r \partial t}\right\} \quad (18)$$

$$S_{zz} + \lambda_1^*\left(\frac{\partial S_{zz}}{\partial t} - 2\frac{\partial w}{\partial r}S_{rz}\right) = -2\frac{\lambda_2^*}{\mathrm{Re}}\left(\frac{\partial w}{\partial r}\right)^2 \quad (19)$$

and

$$-\frac{\partial p}{\partial z} = A^*\cos(\omega^* t) \quad 0 \le t \le T^* \quad (20)$$

equations to be solved for $0 \leqslant \mathrm{r} \leqslant 1$.

3.0.1. Remark 1. When some parameters are set to zero, each model reduces to the newtonian one and an analytical solution can be found [29]:

$$w_n(r,\ t) = -i\frac{A^*}{\omega^*}\mathrm{e}^{i\omega^* t}\left[1 - \frac{J_0(r\sqrt{-i\omega^*\mathrm{Re}})}{J_0(\sqrt{-i\omega^*\mathrm{Re}})}\right] \quad (21)$$

(nondimensional *Womersley solution*), where i is the imaginary unit and j_0 denotes the Bessel function of the first kind, zero order and complex argument†

The constant $\sqrt{\omega^*\mathrm{Re}}$ is a nondimensional parameter characterizing kinematic similarities in oscillating flows (*Womersley number*). For small values of it, as happens in the microcirculation, the Bessel function can be expanded in series and retaining only the quadratic terms, we obtain:

$$w_n(r,\ t) \simeq -i\frac{A^*}{\omega^*}\mathrm{e}^{i\omega^* t}\left[1 - \frac{1 + \frac{i\omega^*\mathrm{Re}r^2}{4}}{1 + \frac{i\omega^*\mathrm{Re}}{4}}\right]$$

and, returning to the real part,

†Similarly, an exact solution if available for the Maxwell fluid (model OB with $\lambda_2^* = 0$) [25].

$$w_n(r,\ t) \simeq \frac{A^*\mathrm{Re}(1-r^2)}{4}\cos(\omega^* t)$$

The velocity is in phase with the pressure distribution, the amplitude being a quadratic function of the radius as is in the steady case [30].

3.0.2. Remark 2. Note that Equations (16) and (19) have no spatial derivative in S_{zz} and the solution can be found numerically at each time step once the values for w and S_{rz} are known.

3.0.3. Remark 3. In the GN case, we have:

$$S_{rz} = \frac{1}{\mathrm{Re}}\left[\gamma + (1-\gamma)\frac{1+\log\delta}{\delta}\right]\frac{\partial w}{\partial r} \qquad S_{zz} = 0 \tag{22}$$

4. NUMERICAL METHOD

Equation (13) or the systems of P.D.E.s (14) and (15) are rewritten as:

$$\frac{\partial \phi}{\partial t} = L(\phi) \tag{23}$$

where ϕ denotes the generical dependent variable/s and L is the generical nonlinear differential operator for spatial terms. The P.D.E. [Equation (23)] is thus split into two subsequent differential problems consisting first in discretizing the spatial operator L with an accurate and efficient method, and then in integrating a system of O.D.E.s in time with a low order finite difference scheme (*method of lines* or *semi-discretization*) [33,34]. Due to the stronger dependence on the space variables, the higher order and the nonlinearities, the spatial operator L requires a different treatment with respect to the time operator.

4.0.1. Space discretization. A spectral collocation method has been used to discretize the spatial operator L [33–37].

The unknown function ϕ is approximated by a truncated series of polynomials $p_k \in \mathbf{P}_n$, where $\mathbf{P}_n$ is the space of polynomials of degree $k \leqslant n$:

$$\phi \approx p = \sum_{k=0}^{n} c_k p_k \tag{24}$$

Let us denote with η_i, $1 \leqslant \mathrm{i} \leqslant n-1$ the zeroes of the derivative of the orthogonal Legendre polynomial of degree n in $[-1, 1]$, and $\eta_0 = -1$, $\eta_n = 1$ the extrema points (Legendre Gauss–Lobatto points). If a representation for p is used in the physical space [canonical Lagrange basis with respect to the set of $(\eta_i)_{i\,=\,0,\ldots,n}$], we have:

$$p(x) = \sum_{k=0}^{n} p(\eta_i) l_k(x) \quad i = 0, \ldots, n \tag{25}$$

where the basis (l_k) is such that:

$$l_k(\eta_i) = \delta_{ki}$$

Expressions for derivatives with respect to the same basis are easily obtainable by replacing coefficients in Equation (25) with other tabulated values [35].

Equation (23) is then replaced by rescaling the operator L in $[-1, 1]$ and by collocating ϕ at $(\eta_i)_{i\,=\,0,\ldots,n}$, that is:

$$\frac{\partial \phi}{\partial t}(\eta_i) = L(\phi(\eta_i)) \quad i = 0, \ldots, n \tag{20}$$

and boundary conditions are imposed at η_0 and η_n.

4.0.2. Time integration. Once an approximate solution is written down as Equation (24), the problem is reduced to solving the system of first order O.D.E.s:

$$\frac{\mathrm{d}\phi_i}{\mathrm{d}t} = L(\phi_i(t)) \quad \text{with} \quad \phi_i = \phi(\eta_i) \qquad i = 0, \ldots, n \tag{27}$$

We choose the following implicit finite difference scheme for solving the system [Equation (27)]:

$$\phi_i^{k+1} - \phi_i^k = \Delta t(1-\theta)L(\phi_i^k) + \Delta t\theta L(\phi_i^{k+1}) \quad i = 0, \ldots, n \tag{28}$$

where the new solution is computed at time $t = (k+1)\Delta t$ and θ is a parameter chosen to control the degree of implicitness and hence the stability of the scheme (θ-*method*). It has been proved that Equation (28) is unconditionally stable if $0.5 \leqslant 0 \leqslant 1$ and is second order accurate for $\theta = 0.5$ [33]. The accuracy reached by the spectral method is slightly reduced by the θ-*method*.

If the spatial operator is nonlinear, as in Equation (13), we replace it by a linear one according to the following iterative scheme:

$$L_\Delta(\phi) = A(\phi)^h \left(\frac{1}{r}\frac{\partial\phi}{\partial r}\right)^{h+1} + B(\phi)^h \left(\frac{\partial^2\phi}{\partial r^2}\right)^{h+1}$$

where $A(\phi)^h$ and $B(\phi)^h$, computed explicitly, are the terms between square brackets in Equation (13): the iteration proceeds until convergence is reached. Such linearization of L is devised in such a way that only the terms corresponding to the laplacian operator L_Δ have been discretized implicitly at time $k+1$, so that the problem (27) is well posed [33].

In the case of linear system [Equations (14)–(16)], the first two components of ϕ are computed simultaneously at each time step. Then, a value for S_{zz} is obtained by solving Equation (16).

Finally the nonlinear system [Equations (17)–(19)] is solved by linearized iterations, similarly to Equation (13), with the term $[\gamma + (1-\gamma)(1 + \log\delta)/\delta]$ computed explicitly.

An initial condition consistent with the boundary conditions has to be chosen: as a reference case, we used the exact solution in the newtonian case [Equation (21)] at $t = 0$. The effect of it disappears after a few (say three) cycles when the flow periodicity is fully developed. Actually the numerical experiments ran over three periods (more in GOB case) revealing a periodic solution after an initial transient†

The coefficients $p(\eta_i)$ in Equation (25) are then computed at each time step as a solution of the algebraic linear system of order $n+1$:

$$(I - \Delta t\theta L_\Delta)\phi_i^{k+1} = (I + \Delta t(1-\theta)L)\phi_i^k \quad i = 0, \ldots, n \tag{29}$$

This is the major time-consuming step in the integration procedure, because of the iteration loop within each time step: the system has been solved by a LU factorization of the matrix of the coefficients with partial pivoting (routine F04AAF–NAG Library). Other more efficient ways to solve it are worth investigating.

Note that the same set of collocation points (η_i) is chosen at each time step and the solution is computed by interpolation over a set of equidistributed points.

5. RESULTS

Once the problem has been formulated in a nondimensional form and a numerical scheme has been implemented as in the former section, the many parameters have been fixed to some likelihood to the blood flow: some of them are typical of physiological measurements and are

†Note that if $\omega^* = 0 \Rightarrow -\partial p/\partial z = A^* = \text{const}$ in Equation (20), the solution tends asymptotically to a steady flow (Hagen–Poiseuille flow in the newtonian case—see Ref. [30]).

chosen to obtain a velocity waveform with characteristic similar to the artery velocity pulses, some others are taken from literature [1,5,17,38]:

$$\rho = 1.05\,\mathrm{g\,cm^{-3}} \quad \eta_0 = 180\,\mathrm{cP} \quad \eta_\infty = 3.96\,\mathrm{cP}$$
$$\Lambda = 53.22\,\mathrm{sec} \quad \lambda_1 = 0.8\,\mathrm{sec} \quad \lambda_2 = 0.2\,\mathrm{sec}$$

The following physical parameters are assigned:

$$\omega = 8\,\mathrm{sec^{-1}} \quad R = 0.1\,\mathrm{cm} \quad W = 1\,\mathrm{cm\,sec^{-1}}$$

$$A = 2600\,\mathrm{cm\,sec^{-2}} \quad T = 3\frac{2\pi}{\omega}\,\mathrm{sec} \simeq 2.35\,\mathrm{sec}$$

The time step has been chosen as $\Delta t = TW/2400R \backsimeq 1.E^{-3}$ and the solution is computed over $n = 20$ collocation points. With this set of parameters the values of the Reynolds and the

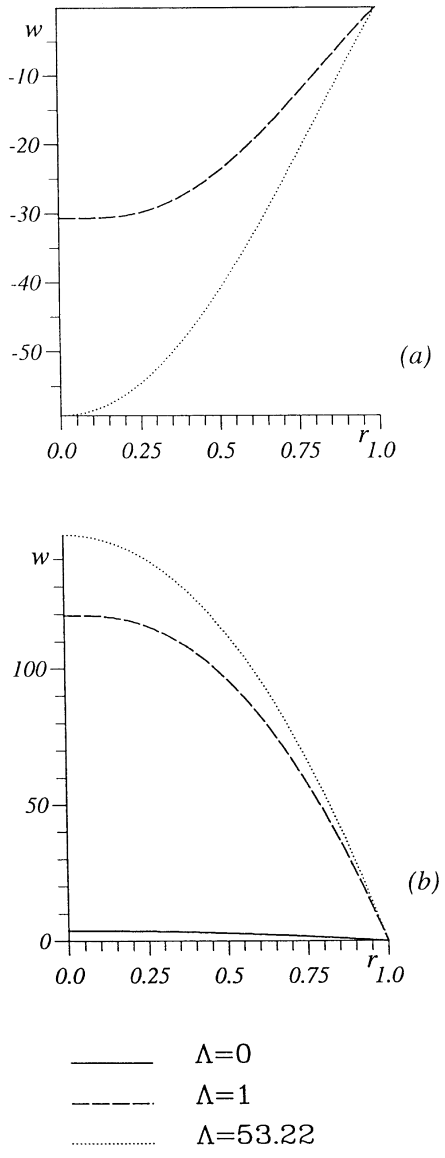

Fig. 2. Nondimensional velocity profiles for model GN at times t_a and t_b.

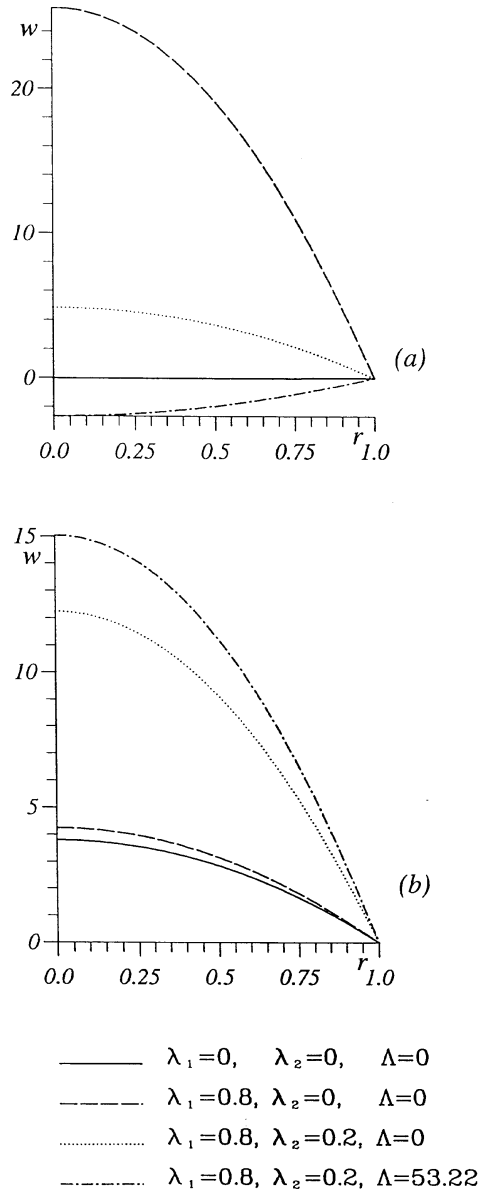

Fig. 3. Nondimensional velocity profiles for model GOB at times t_a and t_b.

Womersley numbers are within the physiological range of blood flow in small vessels [1,17] ($\mathrm{Re} \leqslant 3$ and $\sqrt{\omega^* \mathrm{Re}} \leq 2$).

The numerical solution obtained setting $\lambda_1 = \lambda_2 = \Lambda = 0$ is compared with the exact solution [Equation (21)] in the case of Navier–Stokes fluid, to give some estimate on the accuracy and stability of the numerical scheme. A good agreement is obtained ($\|e\|_\infty \leqslant 1.E^{-4}$). Then, we allow one parameter to change at a time to understand the flow response and its sensitivity to the variation on the physiological and rheological features.

Figures 2 and 3 show the nondimensional velocity profiles in the last cycle (that is after the solution has become periodic) at times $t_a = \frac{11}{12}T$ and $t_b = T$. In the pure shear-thinning fluid there is a considerable increase of velocity with Λ at any time. Also the variation of λ_1 and λ_2 increases the velocity (but with a different order of magnitude or with different sign), and when the three parameters are changed at the same time, then the profile may appear

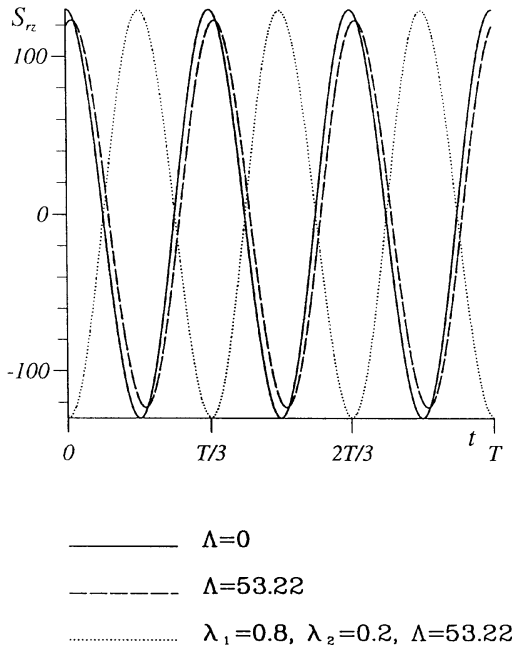

Fig. 4. Nondimensional wall shear stress as a function of time for model GN/GOB.

reversed. Sometimes the shear-thinning effect amplifies that of the viscoelasticity, other times hinders it.

Since the magnitude and the variation of the shear stress at the wall is relevant for the localization and prediction of diseases in blood vessels, the time history in the last three cycles is plotted in Fig. 4. It has been shown that if the shear stress reaches a value >400 dyne cm^{-2} the endothelial surface is irreversibly damaged, and this might be a factor in atherogenesis [1]. The results obtained demonstrate a slight reduction in amplitude and a phase shift in the case $\Lambda \neq 0$. Moreover, in viscoelastic cases, the shear stress has a phase lead ($\simeq 180^\circ$) over that in the inelastic cases, but its magnitude stays under thecritical value for all times. No difference is shown in OB and GOB cases. Moreover the shear stress, as a function of r, can reverse its direction while center line velocities do not.

While in GN fluid $S_{zz}=0$ [cf. Equation (22)], in OB and GOB fluids the normal stress S_{zz} is not zero and can reach an order of magnitude larger than the shear stress and is the most sensitive to the variation of parameters (see Fig. 5).

The flow rate at each instant is computed as:

$$Q = \int_0^1 2\pi r w \mathrm{d}r$$

In Figs 6 and 7 the time histories of Q are shown for many values of the parameters. An increase of Λ causes a noticeable increase of the amplitude, while both amplitude and phase change along λ's and Λ. Note the different scale for Q in GN and GOB fluids.

These results are in accordance with those in Ref. [21] where a first analysis has been developed and a comparison with real data coming from measurements has been carried out.

6. CONCLUSIONS

Three non-newtonian models have been used to study the one dimensional flow in a cylindrical pipe, in order to simulate the blood flow in a straight arterial segment. The deformability of the vascular wall has been disregarded and hence, as a first approximation, the arterial wall has

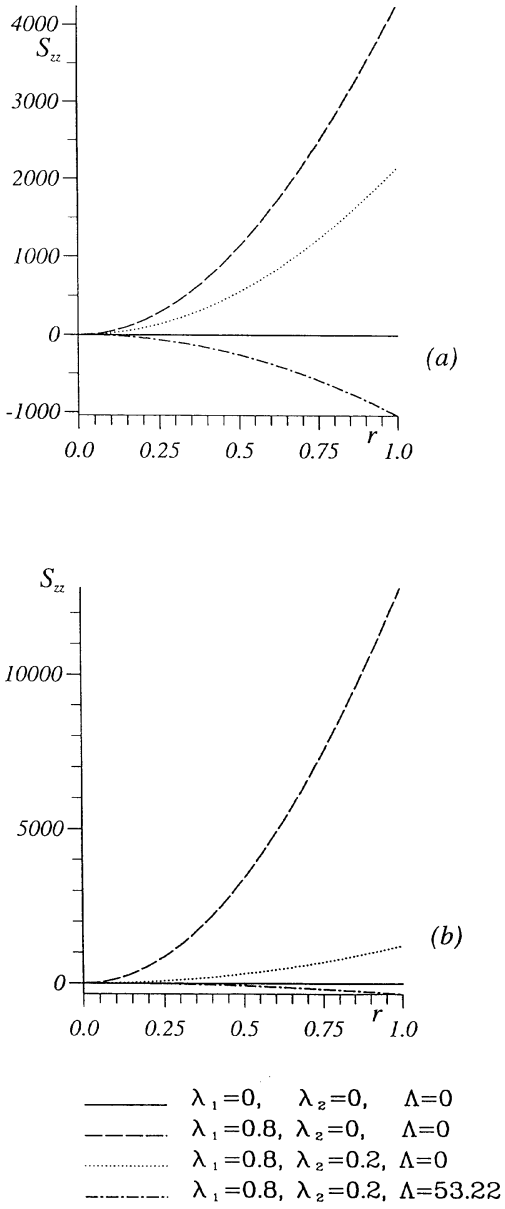

Fig. 5. Nondimensional normal stress S_{zz} for model GOB at times t_a and t_b.

been considered rigid. This is not the case of the real blood vessels, which are elastic and vary their diameter during the cardiac cycle. However, if the relative change in the diameter is of the order of 10%, the error of magnitude made by assuming a fixed diameter is small.

Whereas on the one hand the problem studied may appear to be quite simplified and strongly idealized to model the flow in the cardiovascular system, on the other hand it is a necessary benchmark to analyze the capabilities of the presented models in the blood flow without other spurious effects. This has revealed to be extremely useful in having confidence with the many parameters which it depends on, in a better understanding of the mutual relation between the forces concurrent to the motion and as a starting point for more realistic flows. Non-newtonian models in blood circulation have been revealed as extremely useful in small vessels as they predict peculiar features different from the newtonian cases, reducing to the classical newtonian model in larger vessels where the Reynolds number is higher.

The spectral method has been successfully used for solving a nonlinear system of P.D.E.s after a suitable linearization. Velocity profiles and shear stress along walls have been computed

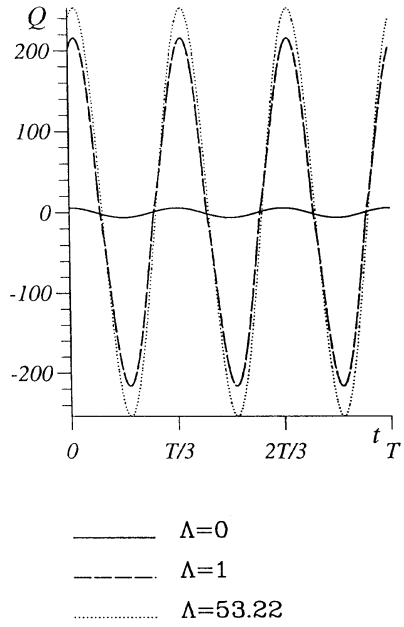

Fig. 6. Nondimensional flow rate as function of time for GN model.

and plotted. For particular values of the parameters, the results match close to those predicted by the Womersley theory in oscillatory flows. The values of the three parameters characterizing the models presented are derived both from rheological considerations and from other studies and have to be carefully identified in order to obtain the best fitting with experimental data: this provides insight on the reliability of each model.

Future work needs to be directed to study the flow of blood in a vessel with a variable (though axisymmetric) section, for example with a stenosis, a bifurcation, and to identify the model parameters through comparison with actual experimental data: these studies can probably give a better understanding of the relationship between fluid dynamics of a pulsatile blood flow and arterial disease.

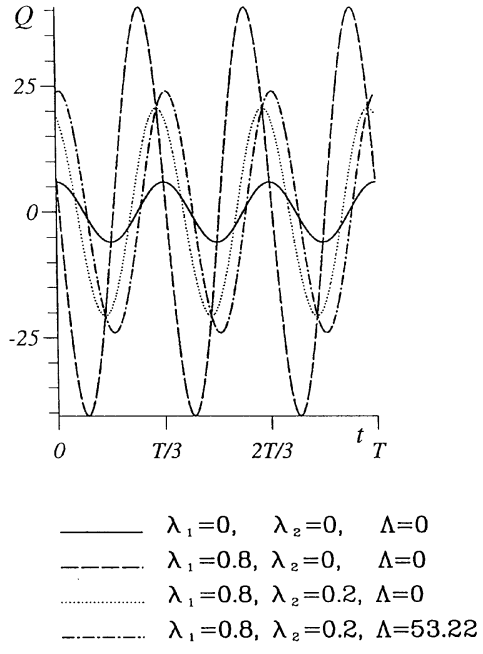

Fig. 7. Nondimensional flow rate as function of time for GOB model.

Acknowledgements—The author wishes to thank Professor K. R. Rajagopal for stimulating discussion about the presented models. We also thank Dr M. Grigioni of the Istituto Superiore di Sanità of Rome for reading the manuscript and for his valuable comments.

REFERENCES

1. T. J. Pedley, *The Fluid Mechanics of Large Blood Vessels*, Cambridge University Press, Cambridge, 1980.
2. Goldsmith, H. L. and Skalak, R., Hemodynamics. *Ann. Rev. Fluid Mech*., 1975, **7, 213–247.**
3. Nerem, R. M., Vascular fluid mechanics, the arterial wall, and atherosclerosis. *ASME J. Biomech. Engineering*, 1992, **114, 274–282.**
4. Friedman, M. H. *et al*.,, Effects of arterial compliance and non–newtonian rheology on correlations between intimal thickness and wall shear. *ASME J. Biomech. Engineering*, 1992, **114, 317–320.**
5. Y. C. Fung, *Biodynamics: Circulation*. Springer-Verlag, New York, 1984.
6. C. Oiknine, Rheology of the human blood. In *Adv. Cardiovasc. Phys*., Vol. 5. Karger, Basel, 1983, pp. 1–25.
7. R. L. Whitmore, *Rheology of the Circulation*. Pergamon Press, Oxford, 1968.
8. R. Pietrabissa and F. Inzoli, Computational analysis of the fluid dynamics of pulsatile flow in an elastic tube. In *XIVth Congress Int. Soc. Biomechanics, Paris*, 4–8 July 1993.
9. Phillips, W. M. and Deutsch, S., Toward a constitutive equation for blood. *Biorheology*, 1975, **12, 383–389.**
10. Chmiel, H., Anadere, I. and Walitza, E., The determination of blood viscoelasticity in clinical hemorheology. *Biorheology*, 1990, **27, 883–894.**
11. Deutsch, S., Phillips, W. M. and Heist, J., An interpretation of low strain rate blood viscosity measurements: a continuum approach. *Biorheology*, 1976, **13, 297–307.**
12. Misra, J. C. and Sahu, B. K., Propagation of pressure waves through large blood vessels: a mathematical model of blood viscoelasticity. *Math. Comp. Modell*., 1989, **12**(3), 333–349.
13. Mann, D. E. and Tarbell, J. M., Flow of non–newtonian blood analog fluids in rigid curved and straight artery models.. *Biorheology*, 1990, **27, 711–733.**
14. G. R. Cokelet, The rheology of human blood. In *Biomechanics: its Fundation and Objectives*, ed. Y. C. Fung, N. Perrone and M. Anliker. Prentice-Hall, Englewood Cliff, 1972, pp. 63–104.
15. Thurston, G. B., Effect of viscoelasticity of blood on wave propagation in the circulation. *J. Biomechanics*, 1976, **9, 13–20.**
16. S. Chien, S. Usami and R. Skalak, Blood flow in small tubes. In *American Physiology Society Handbook of Physiology, Section 2, The cardiovascular system*, Vol. 4. Renkins, Bethesda, MD, 1984, pp. 217–249.
17. W. W. Nichols and M. F. O'Rourke, *McDonald's Blood Flow in Arteries*, Edward Arnold, Sevenoaks, Kent 1990.
18. Perktold, K. and Rappitsch, G., Computer simulation of local blood flow and vessel mechanics in a compliant carotid artery bifurcation model. *J. Biomech*, 1995, **28**(7), 845–856.
19. N. Casson, A flow equation for pigment-oil suspensions of the printing ink type. In *Rheology of Disperse Systems*, ed. Mill. Pergamon, Oxford, 1959.
20. W. M. Phillips, Modelling of flows in the circulatory system. In *Adv. Cardiovasc. Phys*., Vol. 5. Karger, Basel, 1983, pp. 26–48.
21. K. K. Yeleswarapu, Evaluation of continuum models for characterizing the constitutive behavior of blood. Ph. D. Thesis. University of Pittsburgh, Pittsburgh, 1996.
22. K. R. Rajagopal, personal communications, 1996.
23. Ling, S. C. and Atabek, H. B., A nonlinear analysis of pulsatile flow in arteries. *J. Fluid Mech*., 1972, **55, 493–511.**
24. Balmer, R. T. and Fiorina, M. A., Unsteady flow of an inelastic power-law fluid in a circular tube. *J. Non–newtonian Fluid Mech*., 1980, **7, 189–198.**
25. Rahaman, K. D. and Ramkissoon, H., Unsteady axial viscoelastic pipe flows. *J. Non-newtonian Fluid Mech*., 1995, **57, 27–38.**
26. Reddy, J. N. and Padhye, V. A., A penalty finite element model for axisymmetric flows of non-newtonian fluids. *Num. Meth. Part. Diff. Eq*., 1988, **4, 33–56.**
27. Ramkissoon, H., Easwaran, C. V. and Majumdar, S. R., Unsteady flow of an elastico-viscous fluid in tubes of uniform cross-section. *Int. J. Non-linear Mech*., 1989, **24**(6), 585–597.
28. Waters, N. D. and King, M. J., The unsteady flow of an elastico-viscous liquid in a straight pipe of circular cross section. *J. Phys. D*, 1971, **4, 204–211.**
29. Womersley, J. R., Method for the calculation of velocity, rate of flow and viscous drag in arteries when the pressure gradient is known. *J. Physiol*., 1955, **127, 553–563.**
30. G. K. Batchelor, *An Introduction to Fluid Dynamics*. Cambridge University Press, Cambridge, 1967.
31. R. B. Bird, R. C. Armstrong and O. Hassager, Dynamics of Polymeric Liquids, *Vol. 1, Fluid Mechanics*, Wiley, Chichester, 1987.
32. Oldroyd, J. G., On the formulation of rheological equations of state. *Proc. R. Soc. London A*, 1950, **200, 523–541.**
33. C. Canuto, M. Y. Hussaini, A. Quarteroni and T. A. Zang, *Spectral Method in Fluid Dynamics*, Springer Series Comp. Phys. Springer-Verlag, Berlin, 1987.
34. Xu, S., Davies, A. R. and Phillips, T. N., Pseudospectral method for transient viscoelastic flow in an axisymmetric channel. *Num. Meth. Part. Diff. Eq*., 1993, **9, 691–710.**
35. D. Funaro, Polynomial Approximation of Differential Equations, *Lect. Not. Phys*., Springer-Verlag, Berlin, 1992.
36. D. Funaro, *FORTRAN Routines for Spectral Methods*, Pubbl. Preprint n-891, IAN-C.N.R, Pavia, Italy, 1993.
37. Phillips, T. N., On the potential of spectral methods to solve problems in non-newtonian fluid mechanics. *Num. Meth. Part. Diff. Eq*., 1989, **5, 35–43.**
38. S. O. Wille, Finite Element Simulations of the Pulsatile blood flow patterns in arterial abnormalities. In *Finite Elements in Biomechanics*, ed. Gallagher *et al*.. Wiley, Chichester, 1982.